Check for updates

Dynamic Changes in the Levels of Amyloid-β_{42} Species in the Brain and Periphery of APP/PS1 Mice and Their Significance for Alzheimer's Disease

Liding Zhang[1,2], Changwen Yang[1,2], Yanqing Li[1,2], Shiqi Niu[1,2], Xiaohan Liang[1,2], Zhihong Zhang[1,2,3], Qingming Luo[1,2,3] and Haiming Luo[1,2]*

[1] Britton Chance Center for Biomedical Photonics, Wuhan National Laboratory for Optoelectronics, Huazhong University of Science and Technology, Wuhan, China, [2] MoE Key Laboratory for Biomedical Photonics, School of Engineering Sciences, Huazhong University of Science and Technology, Wuhan, China, [3] School of Biomedical Engineering, Hainan University, Haikou, China

Although amyloid-β_{42} (Aβ_{42}) has been used as one of the core biomarkers for Alzheimer's disease (AD) diagnosis, the dynamic changes of its different forms in the brain, blood, and even intestines and its correlation with the progression of AD disease remain obscure. Herein, we screened Aβ_{42}-specific preferred antibody pairs 1F12/1F12 and 1F12/2C6 to accurately detect Aβ_{42} types using sandwich ELISA, including total Aβ_{42}, Aβ_{42} oligomers (Aβ_{42}Os), and Aβ_{42} monomers (Aβ_{42}Ms). The levels of Aβ_{42} species in the brain, blood, and intestines of different aged APP/PS1 mice were quantified to study their correlation with AD progression. Total Aβ_{42} levels in the blood were not correlated with AD progression, but Aβ_{42}Ms level in the blood of 9-month-old APP/PS1 mice was significantly reduced, and Aβ_{42}Os level in the brain was significantly elevated compared to 3-month-old APP/PS1, demonstrating that the levels of Aβ_{42}Ms and Aβ_{42}Os in the blood and brain were correlated with AD progression. Interestingly, in 9-month-old APP/PS1 mice, the level of Aβ_{42} in the intestine was higher than that in 3-month-old APP/PS1 mice, indicating that the increased level of Aβ_{42} in the gastrointestinal organs may also be related to the progression of AD. Meanwhile, changes in the gut microbiota composition of APP/PS1 mice with age were also observed. Therefore, the increase in Aβ derived from intestinal tissues and changes in microbiome composition can be used as a potential early diagnosis tool for AD, and further used as an indicator of drug intervention to reduce brain amyloid.

Keywords: Alzheimer's disease, blood Aβ_{42}, intestinal Aβ, dynamic distribution, ELISA – enzyme-linked immunosorbent assay

INTRODUCTION

Alzheimer's disease (AD) is an age-related, irreversible form of dementia that affects nearly 50 million people worldwide (Collaborators, 2019). A defining pathological feature of AD is the presence of extracellular deposits of aggregated amyloid-β (Aβ) in the form of senile plaques in specific brain tissues and vascular walls (Murphy and LeVine, 2010), the main components of

which are the peptide isoforms $A\beta_{40}$ and $A\beta_{42}$, of which $A\beta_{42}$ predominates in neuritic plaques of AD (Gu and Guo, 2013; Hong and Yaqub, 2019). Autopsy and $A\beta$ positron emission tomography (PET) have indicated that $A\beta$ deposition precedes cognitive decline by a decade or more (Driscoll et al., 2006; Sperling et al., 2011; Oxtoby et al., 2018). $A\beta$, a 4–4.5 kDa peptide containing 39–42 residues, is produced by sequential proteolytic cleavage of amyloid precursor protein (APP), which is expressed in brain cells and peripheral tissues (such as adrenal gland, kidney, heart, liver, spleen, muscles, and blood vessels) (Roher et al., 2009). Considering that skeletal muscle, accounting for 40% of total body weight (Kim et al., 2016), is only one of many peripheral sources of $A\beta$, peripheral $A\beta$ may account for a large portion of total $A\beta$. As observed in human and animal models, brain-derived $A\beta$ peptides can be transported from the brain to peripheral blood (Roberts et al., 2014; Xiang et al., 2015). The communication between the periphery organs and the brain allows for active and dynamic $A\beta$ exchange in distinct reservoirs. The brain accumulation of $A\beta$ aggregates is affected by the levels of $A\beta_{42}$ in the brain and peripheral tissues, but the contribution of peripheral $A\beta$ toward the progression of AD is poorly understood.

$A\beta_{42}$ monomers ($A\beta_{42}$Ms), mainly α-helical and random coil structures, easily aggregate to form various soluble oligomers. The transition of monomers to oligomers triggers the aggregation and pathogenic transformation of $A\beta$ peptides (Nag et al., 2011). A high concentration of $A\beta_{42}$ peptide promotes the formation of its aggregates from soluble monomers into toxic $A\beta_{42}$ oligomers ($A\beta_{42}$Os), and eventually forms extracellular neurotoxic plaques. It has been shown that the brain level of $A\beta_{42}$ increases in the early stage of AD, but decreases with the decline of cognitive ability in the late-stage AD (Naslund et al., 2000). The balance between $A\beta$ production and clearance determines the concentration of $A\beta$ in various reservoirs (Wang et al., 2006). Increasing evidence has implicated that diffusible and soluble $A\beta$ oligomers (Bernstein et al., 2009), rather than insoluble fibrils and small monomers, are the main form of neurotoxicity. These oligomers induce neurotoxic intracellular signaling pathways such as neuronal injury (Wang W. et al., 2019), inflammatory (Salminen et al., 2008), mitochondrial dysfunction, and oxidative stress (Mucke and Selkoe, 2012). The fluctuation of amyloid subtypes in cerebrospinal fluid and blood mainly depends on $A\beta_{42}$Ms and $A\beta_{42}$Os, which are used as core biomarkers to reflect the progression of AD (Benilova et al., 2012). Therefore, dynamic measurement of the levels and profile of $A\beta_{42}$Ms and $A\beta_{42}$Os in the brain and periphery is crucial for studying their physiological metabolism and their substantial correlation with AD progression.

The reliable detection of $A\beta_{42}$Ms and $A\beta_{42}$Os is technically challenging because $A\beta_{42}$Os are transient, heterogeneous, and in dynamic equilibrium with $A\beta_{42}$Ms. In this study, we screened two sequence- and conformation-specific antibodies 1F12 and 2C6, that recognize different epitopes of $A\beta_{42}$. The preferred antibody pairs 1F12/2C6 and 1F12/1F12 were chosen to evaluate the potential significance of various sources and pools of $A\beta_{42}$ on the overall pathology of AD. The correlation between blood $A\beta_{42}$ levels and brain $A\beta_{42}$ levels in APP/PS1 and

age-matched C57BL/6J mice at 3 and 9 months was dynamically assessed. Another comprehensive longitudinal study determined the potential effects of intestinal tissue-derived $A\beta_{42}$ on blood and brain $A\beta_{42}$ levels in APP/PS1 mice. We expect that our research will promote the understanding of the role of $A\beta_{42}$Ms and $A\beta_{42}$Os in the progression of AD.

MATERIALS AND METHODS

Chemicals and Materials

The $A\beta_{3-9}$, $A\beta_{13-19}$, $A\beta_{18-25}$, $A\beta_{29-36}$, $A\beta_{36-42}$, $A\beta_{40}$, and $A\beta_{42}$ were custom-synthesized as lyophilized powders by Royo Biotech Co., Ltd (Shanghai, China) with a purity of >95%. Anti-$A\beta$ (6E10) antibody was obtained from Invitrogen. The goat anti-mouse IgG (H + L), protein A resin, and protein L resin were ordered from GenScript (Nanjing, China). The mouse monoclonal antibody isotyping kit was purchased from Southern Biotech (Birmingham, AL, United States). The Pierce streptavidin-coupled poly-HRP and protein marker were ordered from Thermo Scientific (Massachusetts, United States). Thioflavin S, BSA, Freund's complete adjuvant, and Freund's incomplete adjuvant were obtained from Sigma-Aldrich. Cy3-NHS ester and Biotin-PEG4-NHS ester were provided by Lumiprobe (Hannover, Germany). All other chemicals were purchased from commercial suppliers and used as received.

Oligomeric and Monomeric $A\beta$ Preparations

The $A\beta_{40}$ monomers ($A\beta_{40}$Ms) and $A\beta_{42}$Ms were obtained by dissolving lyophilized $A\beta_{40}$, $A\beta_{42}$ peptides in 1,1,1,3,3,3-hexafluoroisopropanol (HFIP), followed by incubation overnight at room temperature. HFIP was evaporated with nitrogen gas to form a film, and the $A\beta$ was redissolved in dimethyl sulfoxide. The prepared $A\beta_{40}$, $A\beta_{42}$ monomers solution (50 μM) was stored at $-20°$C as stock solution. The $A\beta_{40}$ oligomers ($A\beta_{40}$Os) and $A\beta_{42}$ oligomers ($A\beta_{42}$Os) were obtained from 24 h incubation of 50 μM $A\beta_{40}$ and $A\beta_{42}$ monomer solutions at 37°C in the dark, respectively.

Cryo-Transmission Electron Microscopy

The patterns of the prepared $A\beta_{42}$Ms and $A\beta_{42}$Os were confirmed by cryo-transmission electron microscopy (Cryo-TEM). In brief, 5 μL of each sample was deposited on a copper grid, and the excess liquid was removed using a filter paper, leaving a thin film of the solution on the grid. The Tecnai G20 transmission electron microscope (FEI Ltd., United States) was used to characterize the morphology of the above-mentioned samples.

Generation and Purification of 1F12 and 2C6

The antigen was prepared using lyophilized synthetic $A\beta_{42}$ peptide dissolved in 10 mM NaOH and diluted with PBS to a final concentration of 1 mg/mL. In the first immunization, BALB/c mice were immunized with 50 μg $A\beta_{42}$ peptide

mixed with Freund's complete adjuvant. In the second and third immunizations, $A\beta_{42}$ peptides and Freund's incomplete adjuvant mixtures were used (Zhang et al., 2018). After the third immunizations, 50 μg $A\beta_{42}$ peptide was used for booster immunization. Three days later, spleen cells were collected from the immunized mice and fused with SP2/0 cells via PEG at 37°C (Wang X. et al., 2019). The fused cells were maintained in HAT medium for 7 days and then cultured in HT medium. The positive hybridomas in each plate were screened by the limited dilution method (Kohler and Milstein, 1975). Three positive hybridoma cell lines were screened from the initial positive wells and cultured to prepare ascites. The immunoglobulins of 1F12, 2C6, and 2E2 were purified using protein A resin, according to the manufacturer's instructions.

Dot Blot Assay

One microgram of each $A\beta_{42}$ truncated peptide including $A\beta_{3-9}$, $A\beta_{13-19}$, $A\beta_{18-25}$, $A\beta_{29-36}$, and $A\beta_{36-42}$ was pipetted onto a PVDF membrane activated by methanol. After the peptide samples were deposited, the PVDF membrane was air-dried and blocked in 5% skimmed milk in phosphate-buffered saline (PBS) with Tween-20 detergent (PBS-T) at 37°C for 1 h. The membranes were then incubated with mAb 1F12 (1:1000) or 2C6 (1:1000) at 37°C for 2 h. After washing three times in PBS-T, the membrane was incubated with the secondary antibody HRP-conjugated goat anti-mouse IgG (H + L) at 37°C for 2 h, and the immunological signals were detected with ECL-substrate (Vazyme, China) using Tanon 5200 Muiti (Shanghai, China).

Biotinylated 1F12 or 2C6 Antibody Preparation

The biotinylated antibodies were generated based on the reaction of amino groups of 1F12 or 2C6 antibody with biotin N-hydroxysuccinimide (NHS) ester. Briefly, 10 nmol of 1F12 or 2C6 antibody was dissolved in PBS, and the solution pH was adjusted to 8.5 with Na_2CO_3 (0.1 M), followed by a reaction with 20 nmol biotin-PEG4-NHS esters in DMSO at room temperature for 2 h. The biotin-modified 1F12 or 2C6 antibody was purified using size exclusion PD-10 columns with PBS as the mobile phase. Indirect ELISA determined the activities and titers of biotinylated 1F12 or 2C6. The indirect ELISA assay was performed using serially diluted biotin-labeled antibodies (from 1:100 to 1:409,600) instead of the primary antibody. After incubation with the Pierce streptavidin-coupled poly-HRP, the immunoreaction was visualized with a soluble TMB substrate solution.

Measurement of the Titer and Binding Affinity of 1F12 or 2C6 Antibody

The 96-well plates were coated with 0.5 μg/well of $A\beta_{42}$ and blocked with 5% skimmed milk dissolved in a PBS-T buffer for 2 h at room temperature. Subsequently, series of diluted 1F12 or 2C6 ranging from 1:100 to 1:409,600 were added into each well for 2-h incubation at 22°C. The subsequent steps were performed as described in the ELISA section above. The binding affinities of 1F12 or 2C6 with $A\beta_{42}$ species were determined using serially

diluted preparations of 1F12 or 2C6 with serials of concentrations (from 10 μg/mL to 10 ng/mL) instead of different dilutions (from 1:100 to 1:409,600). After incubation with the HRP-conjugated goat anti-mouse IgG (H + L), the immunoreaction was visualized with a soluble TMB substrate solution.

Screening of Preferred Antibody Pairs for Total $A\beta_{42}$ and $A\beta_{42}Os$ Sandwich ELISA

Preferred antibody pairs of total $A\beta_{42}$ and $A\beta_{42}Os$ sandwich ELISA were screened from the combination of different antibody pairs. The screening process of antibody pairs for total $A\beta_{42}$ was as follows: 96-well plate was coated with 1 μg/well of 1F12 or 2C6 as the capture antibody for 2 h at room temperature, and then blocked with 5% skimmed milk. Five ng total $A\beta_{42}$ containing $A\beta_{42}Ms$ and $A\beta_{42}Os$ or $A\beta_{42}Os$ was loaded into each well and incubated 2 h at room temperature, followed by the addition of biotinylated 2C6 or 1F12 as the detection antibody. Finally, streptavidin-coupled poly-HRP was used to visualize the immunoreaction of each well.

Sandwich ELISA for the Detection of Total $A\beta_{42}$ and $A\beta_{42}Os$

The 96-well plates were coated with 1 μg/well of 1F12 in the citrate-buffered saline buffer for 2 h, and then blocked with 5% skimmed milk dissolved in PBS-T for 2 h at room temperature. A standard series of synthetic $A\beta$ peptides ($A\beta_{40}Ms$, $A\beta_{42}Ms$, $A\beta_{40}Os$, and $A\beta_{42}Os$) and the biological samples (mouse blood and organ homogenization) to be analyzed were added to the plates in triplicates and incubated for 40 min at room temperature. The plate was washed three times with PBS-T and incubated with biotinylated mAb 2C6 for total $A\beta_{42}$ detection or biotinylated mAb 1F12 for $A\beta_{42}Os$ detection, followed by incubation with streptavidin-coupled poly-HRP for 1 h at room temperature. The immunoreaction in each well was detected using TMB substrate solution.

Quantification of $A\beta$ Peptides in Blood, Brain, and Intestinal Tissue

All procedures involving animal studies were reviewed and approved by the Institutional Animal Care and Use Committee of Huazhong University of Science and Technology. Herein, 3-month-old APP/PS1 mice (six mice for blood collection including three female and three male mice, and four mice for tissue collection, including two female and two male mice), 9-month-old APP/PS1 mice (six mice for blood collection including three female and three male mice, $n = 4$ for tissue collection, including two female and two male mice), and age-matched non-transgenic C57BL/6J mice (six mice for blood collection, including three female and three male mice, and four mice for tissues collection, including two female and two male mice) were anesthetized with 0.4 mL Avertin (25 mg/mL) and intracardially perfused with 0.9% saline solution. The mouse blood was collected, and tissues were organically extracted with antigen extraction tris-buffered saline (TBS, 20 mM Tris and 137 mM NaCl, pH 7.6) at a ratio of 1:50 (w/v) using a tissue grinder. The TBS included a complete protease inhibitor cocktail

(Roche). The supernatant of homogenates was centrifuged at 10,000 g for 30 min in Type 60 Ti fixed angle rotor at 4°C to obtain TBS-soluble proteins. The collected mouse blood, prepared brain, and intestinal tissue samples were used for $A\beta_{42}$ quantification by the above-prepared sandwich ELISA.

Immunoprecipitation and Western Blotting

The homogenates of organ tissues (brain, stomach, duodenum, jejunum, ileum, cecum, colon, and intestinal lysates) or blood were incubated for 30 min at room temperature with 40 μg/mL of 1F12 antibody conjugated on the protein A/G magnetic bead, according to the manufacturer's instructions. The immunoprecipitated proteins were eluted with 0.1 M glycine (pH 3.0) and immediately neutralized to pH 7.4 using a neutralization buffer (1 M Tris-HCl, pH 8.5). The samples were then denatured in loading buffer (Boster Biotech, United States) and boiled for 10 min. Following this, the proteins were run on a 12% reduced tris-tricine SDS-polyacrylamide gel via SDS-PAGE. Proteins were transferred onto a polyvinylidene fluoride membrane at 160 mA for 1 h, at 4°C. Membranes were blocked with 5% skimmed milk dissolved in 1 × PBS-T and incubated with 1F12 or 2C6 for 2 h at 37°C. Subsequently, the membranes were washed in PBS-T followed by 1 h incubation with secondary antibody HRP-conjugated goat anti-mouse IgG (H + L), and the immunological signals were detected using the ECL-substrate (Vazyme, China) on Tanon 5200 Muiti (Shanghai, China).

Immunofluorescence Assays of Tissues

The mice were anesthetized with 0.4 mL Avertin (25 mg/mL), and cardiac perfusion was performed with 4% paraformaldehyde (PFA) for 30 min. The tissues (brain, duodenum, jejunum, ileum, cecum, and colon) from mice were collected, fixed in 4% PFA, and dehydrated in sucrose solution. After embedding in OCT compound (Tissue-Tek; Sakura Finetek, Netherlands, United States), 15 μm coronal frozen sections of tissue samples were serially cut on a Leica CM3050 S cryostat. Each slice was mounted on glass slides and permeabilized with 0.2% Triton X-100 overnight at 4°C. The slice was blocked with 3% BSA for 2 h at room temperature and incubated with thioflavin S or commercially available anti-Aβ antibody 6E10, Cy3-conjugated 1F12 or 2C6 overnight at 4°C. All slides were washed five times with PBS and stained with thioflavin S. The Zeiss LSM710 microscope was used to image slides with red, green, and blue fluorescence filters.

Sequencing Data and Statistical Analyses

Sequencing data from an independent study of the APP/PS1 mice gut microbiota was obtained. Raw 16S sequences were downloaded from SRA accession PRJNA543965 and preprocessed using the 'dada2' R package. Reads were truncated at 150 bp, then a maximum expected error rate threshold of 1 was imposed. Taxonomy was assigned using the Silva v138 rRNA database using the default classify algorithm of dada2 (v1.16.0).

Downstream analysis was performed by several R packages including 'phyloseq,' 'MicrobiotaProcess,' 'DESeq2,' and 'ggplot2.' Beta diversity was measured by principal coordinate analysis (PCoA) based on weighted UniFrac phylogenetic distance. The significantly differed genus between groups was determined using 'DESeq2,' and their significance of difference was assessed by Wilcoxon rank-sum test. The significance cut-off was set at $^*p < 0.05$.

The data, except for sequencing data, are presented as means ± SEM. One-way or two-way analysis of variance (ANOVA) was used for multiple group comparisons. Statistical significance is represented in the figure by $^*p < 0.05$, $^{**}p < 0.01$, $^{***}p < 0.001$, $^{****}p < 0.0001$, and n.s. (indicating no significance). All statistical analyses were performed with GraphPad Prism7.0 software.

RESULTS

Screening and Identification of $A\beta_{42}$ Sequence- and Conformation-Specific Antibodies

BALB/c mice were immunized with human $A\beta_{42}$ peptide preparations, and a pool of approximately 1,500 clones was generated via hybridoma technology. In addition, 75 of these clones reacted with Aβ monomers and oligomers in ELISA (**Supplementary Figure 1A**). Then three positive hybridoma clones 1F12, 2C6, and 2E2 were selected, and their immunoglobulin isotypes were determined. The results showed that the isotype of 1F12 and 2C6 was IgG2a, and the isotype of 2E2 was IgA, and the light chains of these three monoclonal antibodies (mAbs) all belonged to the kappa chain (**Figure 1A**). Reduced SDS-PAGE identified the purity and molecular weight of these three mAbs (**Supplementary Figure 1B**). Therefore, 1F12 and 2C6 were chosen to characterize their reactivity by Western blotting brain natural $A\beta_{42}$ and immunostaining brain slices of APP/PS1 mice. The results displayed strong bands of $A\beta_{42}$ peptides recognized by 1F12 and 2C6, comparable to those obtained with 6E10 (**Supplementary Figure 1C**). Immunofluorescence imaging (using thioflavin S or commercially available anti-Aβ antibody 6E10) showed that Aβ plaques were colocalized with Cy3-labeled 1F12 (**Figure 1B** and **Supplementary Figure 2A**) or 2C6 (**Supplementary Figures 1D, 2B**). The titer of mAbs was determined by indirect ELISA and calculated as 1:204800 for 1F12, 1:102400 for 2C6, 1:51200 for 2E2 (**Supplementary Figure 1E**).

To identify the linear fragments (epitopes) of $A\beta_{42}$ recognized by 1F12 and 2C6, we performed epitope mapping experiments using a series of peptides starting from +3 to +42 in the $A\beta_{42}$ sequence. Based on a series of dot-blot analyses, we observed that 1F12 displayed a linear epitope, amino acids 3–9 located in the N-terminal region of the $A\beta_{42}$ peptide (**Figure 1C**, left). In contrast, 2C6 exhibited discrete epitopes, including four distinct $A\beta_{42}$ fragments (**Figure 1C**, right). To confirm the binding efficacy of 1F12 and 2C6 to $A\beta_{42}$ and $A\beta_{40}$ peptides, indirect ELISAs were performed on separate $A\beta_{42}$ and $A\beta_{40}$ coated plates.
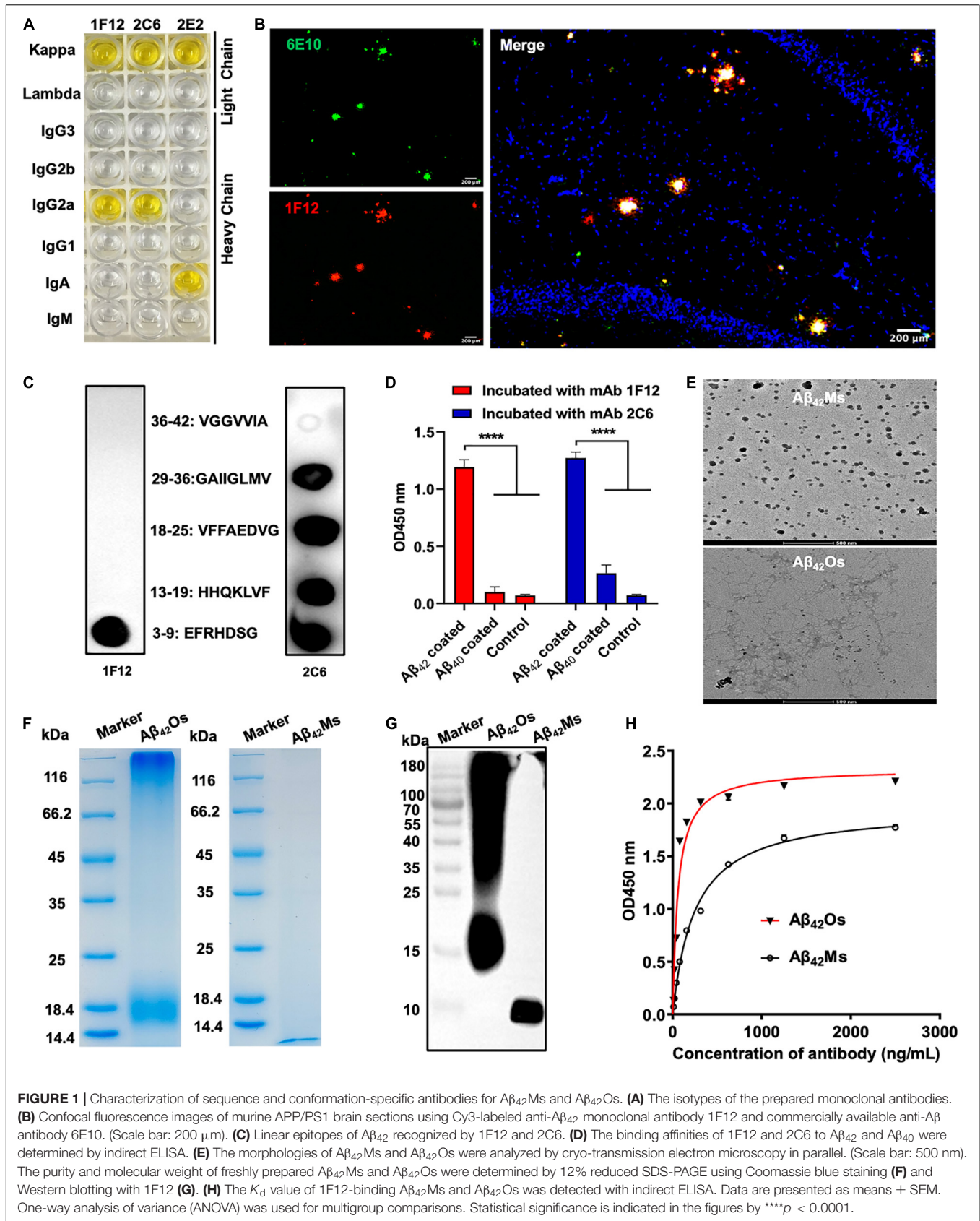
FIGURE 1 | Characterization of sequence and conformation-specific antibodies for Aβ_{42}Ms and Aβ_{42}Os. **(A)** The isotypes of the prepared monoclonal antibodies. **(B)** Confocal fluorescence images of murine APP/PS1 brain sections using Cy3-labeled anti-Aβ_{42} monoclonal antibody 1F12 and commercially available anti-Aβ antibody 6E10. (Scale bar: 200 μm). **(C)** Linear epitopes of Aβ_{42} recognized by 1F12 and 2C6. **(D)** The binding affinities of 1F12 and 2C6 to Aβ_{42} and Aβ_{40} were determined by indirect ELISA. **(E)** The morphologies of Aβ_{42}Ms and Aβ_{42}Os were analyzed by cryo-transmission electron microscopy in parallel. (Scale bar: 500 nm). The purity and molecular weight of freshly prepared Aβ_{42}Ms and Aβ_{42}Os were determined by 12% reduced SDS-PAGE using Coomassie blue staining **(F)** and Western blotting with 1F12 **(G)**. **(H)** The K_d value of 1F12-binding Aβ_{42}Ms and Aβ_{42}Os was detected with indirect ELISA. Data are presented as means ± SEM. One-way analysis of variance (ANOVA) was used for multigroup comparisons. Statistical significance is indicated in the figures by ****$p < 0.0001$.

The 1F12 and 2C6 detection signals of $A\beta_{42}$ were significantly higher than those of $A\beta_{40}$ (**Figure 1D**). Taken together, 1F12 and 2C6 were $A\beta_{42}$ sequence-specific antibodies, and both showed a preference for the conformational epitope presented by $A\beta_{42}$ rather than $A\beta_{40}$.

Binding Affinities and Selectivity of 1F12 and 2C6 for Different $A\beta_{42}$ Species

We further evaluated the binding affinity of 1F12 and 2C6 to $A\beta_{42}$Ms and $A\beta_{42}$Os with different conformations. Cyo-TEM confirmed the morphology of the prepared $A\beta42$Ms and $A\beta42$Os. The results showed that the morphology of $A\beta_{42}$Ms was α-helical and random coil structures (**Figure 1E**, up), while $A\beta_{42}$Os formed a β-sheet and typical fibril three-dimensional structures (**Figure 1E**, down). 12% reduced SDS-PAGE gel confirmed the purity and molecular weight of the prepared $A\beta_{42}$Ms and $A\beta_{42}$Os (**Figure 1F**), and their components were verified by Western blotting (**Figure 1G** and **Supplementary Figure 1F**). Indirect ELISA results showed that the K_d values of 1F12 bound to $A\beta_{42}$ species were 1.66 ± 0.09 nM for $A\beta_{42}$Ms and 0.38 ± 0.04 nM for $A\beta_{42}$Os (**Figure 1H**), while the K_d values of 2C6 were 3.59 ± 0.27 nM for $A\beta_{42}$Ms and 0.61 ± 0.03 nM for $A\beta_{42}$Os (**Supplementary Figure 1G**). Taken together, 1F12 and 2C6 were $A\beta_{42}$ sequence- and conformation-specific antibodies and could bind $A\beta_{42}$ species with different conformations.

Preferred Antibody Pairs for Specific Detection of Total $A\beta_{42}$ and $A\beta_{42}$Os

The screening of capture and detecting antibodies for sandwich ELISA is a prerequisite for developing techniques to detect and quantify $A\beta_{42}$Ms and $A\beta_{42}$Os. Both 1F12 and 2C6 were biotinylated, and indirect ELISA showed that their bioactivities and titers were high (**Supplementary Figures 1H,I**). To achieve the specific detection of total $A\beta_{42}$ and $A\beta_{42}$Os, a combination of different antibody pairs (1F12/2C6, 1F12/2E2, 2C6/1F12, 2C6/2E2, 2E2/1F12, 2E2/2C6) was screened for preferred antibody pairs by comparing their susceptibility to total $A\beta_{42}$ and $A\beta_{42}$Os in sandwich ELISA (**Figure 2A**). The capture/detection antibody pair 1F12/2C6 had the highest detection signal and specificity for total $A\beta_{42}$ among the six antibody pairs in ELISA (**Figures 2B,C**), while the 1F12/1F12 antibody pair was significantly more effective and specificity in detecting $A\beta_{42}$Os (**Figures 2D,E**).

Dynamic Monitoring of Changes in Total $A\beta_{42}$, $A\beta_{42}$Os, and $A\beta_{42}$Ms in Blood and Brain

To dynamically monitor the changes of total $A\beta_{42}$, $A\beta_{42}$Os, and $A\beta_{42}$Ms in the brain and periphery blood, 1F12/2C6 and 1F12/12 ELISAs were performed to quantify $A\beta_{42}$ in peripheral blood and brain extracts of 3 and 9-month-old APP/PS1 mice. The results showed that regardless of age (at 3- or 9-month-old), the total $A\beta_{42}$ in blood and brain extracts of APP/PS1 mice was significantly higher than that in the tissue extracts of C57BL/6J (**Figure 3A**). 1F12/2C6 ELISA showed that compared with the 3-month-old APP/PS1, the total $A\beta_{42}$ levels in the blood of the
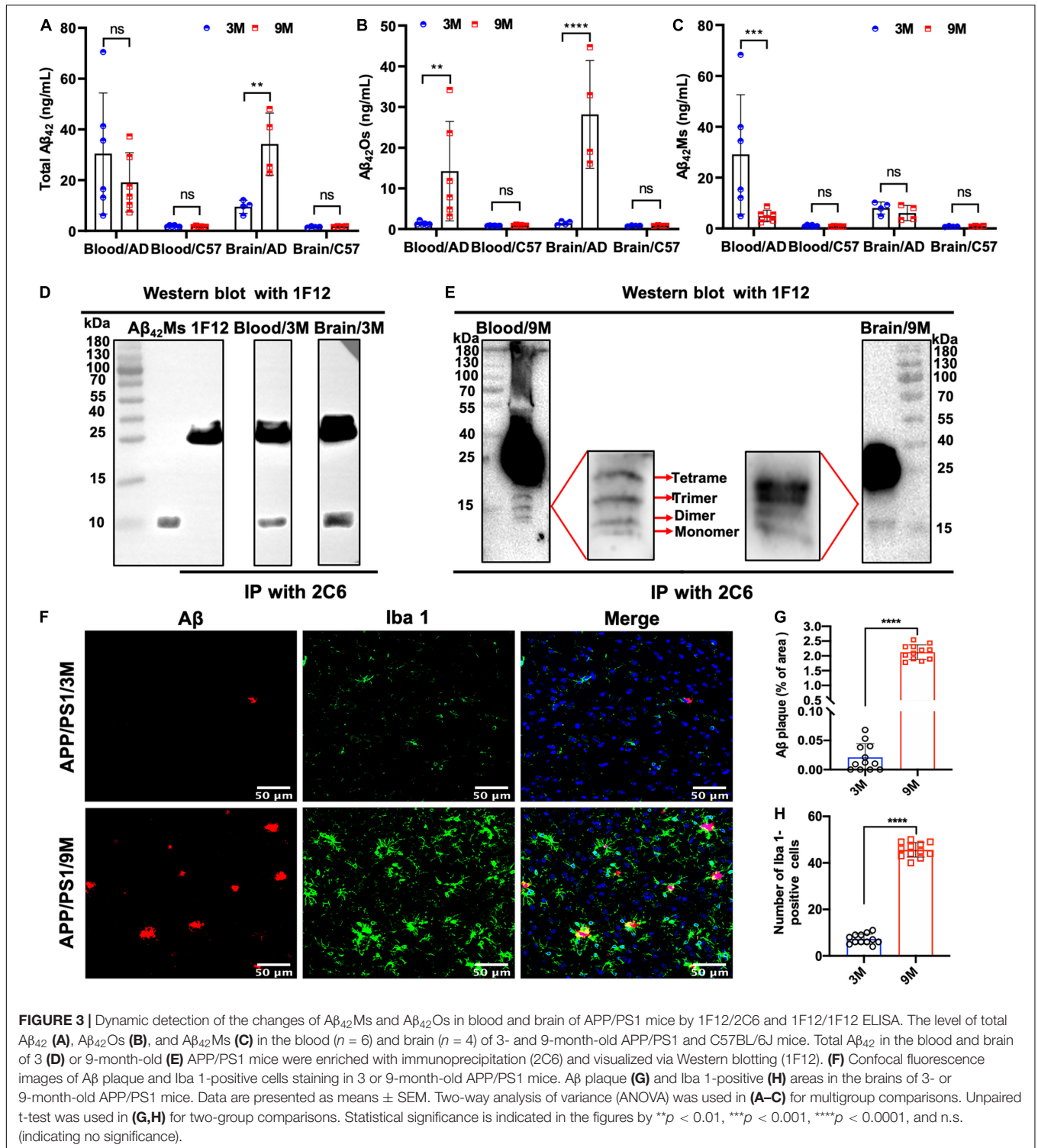
9-month-old APP/PS1 did not change significantly ($p = 0.1787$), but the $A\beta_{42}$ content in the brain tissue was significantly increased ($p = 0.0062$, **Figure 3A**). In comparison, 1F12/1F12 ELISA showed that the $A\beta_{42}$Os level in the blood ($p = 0.005$) and brain ($p < 0.0001$) of APP/PS1 at 9 months old were significantly higher than that of APP/PS1 mice at 3 months old (**Figure 3B**). The amount of $A\beta_{42}$Ms was calculated by subtracting the total $A\beta_{42}$ from $A\beta_{42}$Os. The level of $A\beta_{42}$Ms in the blood of APP/PS1 mice at 9 months old was significantly lower than that of APP/PS1 mice at 3 months old ($p = 0.0004$, **Figure 3C**). The levels of total $A\beta_{42}$, $A\beta_{42}$Os, and $A\beta_{42}$Ms in C57BL/6J mice between 3 and 9 months old did not change significantly (**Figures 3A–C**). To further validate the 1F12/2C6 and 1F12/1F12 ELISA results, an immunoprecipitation (IP) assay was performed using blood and brain extracts of 3- and 9-month-old APP/PS1 mice. As shown in **Figure 3D**, a clear single band was observed in the blood and brain extracts of 3-month-old APP/PS1, and its molecular weight was similar to $A\beta_{42}$Ms. The results were consistent with the ELISA results as above-mentioned, confirming that the level of $A\beta_{42}$Ms at the early stage of AD (3-month-old APP/PS1) was high and the level of $A\beta_{42}$Os in the late stage of AD (9-month-old APP/PS1) were elevated. Western blotting analysis of immunoprecipitated proteins in blood and brain extracts of 9-month-old APP/PS1 mice revealed a prominent $A\beta_{42}$Os band with a molecular weight of more than 5 kDa and several clear bands of monomers to tetramers (**Figure 3E**). Taken together, $A\beta_{42}$ mainly existed as a monomer in the blood at the early stage of AD (e.g., 3-month-old APP/PS1 mice with less $A\beta$ plaque load and Iba 1-positive cells staining, **Figures 3F–H**), whereas it appears as oligomers in blood and brain extracts at the late state (e.g., 9-month-old APP/PS1 mice with more $A\beta$ plaque load and Iba 1-positive cells staining, **Figures 3F–H**).

Correlation of Total $A\beta_{42}$, $A\beta_{42}$Os, and $A\beta_{42}$Ms Level in the Gastrointestinal System With AD Progression

Apart from blood and brain, we also paid attention to the distribution of $A\beta_{42}$ in the intestinal system of APP/PS1 mice, such as duodenum, jejunum, ileum, colon, cecum, and their lysates. Several research groups have reported that AD may begin in the intestine and is closely related to the imbalance of intestinal flora (Hu et al., 2016; Harach et al., 2017; Jiang et al., 2017; Mancuso and Santangelo, 2018). To detect the distribution of total $A\beta_{42}$, $A\beta_{42}$Ms, and $A\beta_{42}$Os in the intestinal systems and explore its potential correlation with the pathogenesis of AD, organs extracted from different parts of intestines (duodenum, jejunum, ileum, colon, and cecum) and their lysates from 3- and 9-month-old APP/PS1 mice were collected for 1F12/2C6 and 1F12/1F12 ELISA. No $A\beta_{42}$ was detected in the different parts of intestines in 3-month-old APP/PS1 mice, but a certain amount of $A\beta_{42}$ was observed in jejunum lysate and colonic lysate (**Figure 4A**). Further analysis revealed $A\beta_{42}$ subtype in the jejunum and colon lysates. It was found that $A\beta_{42}$Os were observed in both jejunum and colonic lysate, with higher levels of $A\beta_{42}$Os in colon lysates (**Figure 4B**). But for $A\beta_{42}$Ms, a weak signal was only observed in the colonic lysate (**Figure 4C**). However, for 9-month-old
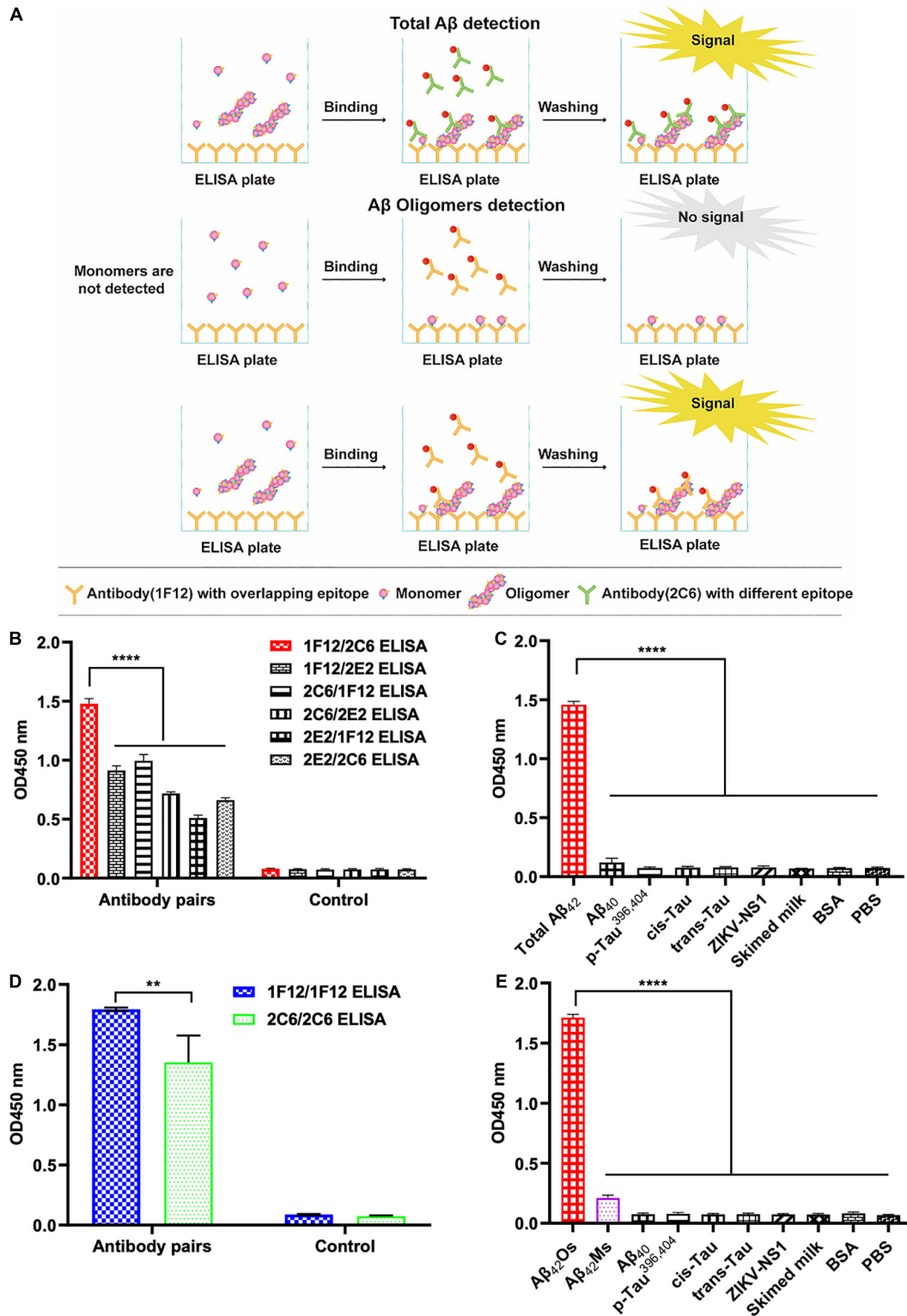
FIGURE 2 | Screening of preferred antibody pairs 1F12/2C6 and 1F12/1F12 against Aβ_{42}Ms and Aβ_{42}Os. **(A)** Schematic representation of 1F12/2C6, 1F12/1F12 ELISA to detect total Aβ_{42}, Aβ_{42}Os, respectively. **(B)** Preferred antibody pairs were screened for the detection of total Aβ_{42}. **(C)** The specificity assay of 1F12/2C6 ELISA for total Aβ_{42} detection. **(D)** Preferred antibody pairs were screened for the detection of Aβ_{42}Os. **(E)** The specificity assay of 1F12/1F12 ELISA for Aβ_{42}Os detection. Data are presented as means ± SEM. Two-way analysis of variance (ANOVA) was used for **(B,D)** and One-way analysis of variance (ANOVA) was used for **(C,E)**. Statistical significance is indicated in the figures by **$p < 0.01$ and ****$p < 0.0001$.

FIGURE 3 | Dynamic detection of the changes of $A\beta_{42}$Ms and $A\beta_{42}$Os in blood and brain of APP/PS1 mice by 1F12/2C6 and 1F12/1F12 ELISA. The level of total $A\beta_{42}$ **(A)**, $A\beta_{42}$Os **(B)**, and $A\beta_{42}$Ms **(C)** in the blood ($n = 6$) and brain ($n = 4$) of 3- and 9-month-old APP/PS1 and C57BL/6J mice. Total $A\beta_{42}$ in the blood and brain of 3 **(D)** or 9-month-old **(E)** APP/PS1 mice were enriched with immunoprecipitation (2C6) and visualized via Western blotting (1F12). **(F)** Confocal fluorescence images of $A\beta$ plaque and Iba 1-positive cells staining in 3 or 9-month-old APP/PS1 mice. $A\beta$ plaque **(G)** and Iba 1-positive **(H)** areas in the brains of 3- or 9-month-old APP/PS1 mice. Data are presented as means ± SEM. Two-way analysis of variance (ANOVA) was used in **(A–C)** for multigroup comparisons. Unpaired t-test was used in **(G,H)** for two-group comparisons. Statistical significance is indicated in the figures by **$p < 0.01$, ***$p < 0.001$, ****$p < 0.0001$, and n.s. (indicating no significance).

APP/PS1 mice, total $A\beta_{42}$ signals were clearly observed in all gastrointestinal organs and their lysates, except for duodenum, duodenum lysates, and colonic lysates (**Figure 4A**). In a detailed analysis, we found that $A\beta_{42}$ mainly existed in the form of oligomers and was detected in all gastrointestinal organs except for the duodenum (**Figure 4B**). For the lysates, the result was opposite to the $A\beta_{42}$Ms level, and only two oligomers were detected with weak signals in the jejunum and ileum lysates (**Figure 4C**). For 3 or 9-month-old C57BL/6J mice, no significant differences were observed in the gastrointestinal organs and their lysates (**Supplementary Figures 3A,D**). Interestingly, the monomeric (**Supplementary Figures 3C,F**) or oligomeric

FIGURE 4 | Dynamic changes in the levels of Aβ_{42}Ms and Aβ_{42}Os in the intestines were detected and quantified via 1F12/2C6 and 1F12/1F12 ELISA. The level of total Aβ_{42}, Aβ_{42}Os, and Aβ_{42}Ms in the stomach, duodenum, jejunum, ileum, colon, and cecum and their lysates from 3-month-old APP/PS1 ($n = 4$; **A–C**), 9-month-old APP/PS1 ($n = 4$; **A–C**). **(D)** Representative IP-Western blotting data to analyze the distribution of Aβ_{42} in the stomach, duodenum, jejunum, ileum, colon, and cecum and their lysates from 3-month-old APP/PS1 (i), 9-month-old APP/PS1 (iii), and C57BL/6J mice (ii,iv) at the same ages. **(E,F)** The Western blotting results for Aβ_{42} in APP/PS1 or C57BL/6J mice were quantified. Data are presented as means ± SEM. Two-way analysis of variance (ANOVA) was used for multigroup comparisons. Statistical significance is indicated in the figures by *$p < 0.05$, **$p < 0.01$, ***$p < 0.001$, and ****$p < 0.0001$.

(**Supplementary Figures 3B,E**) forms of Aβ_{42} levels in APP/PS1 mice were significantly higher than those in the C57BL/6J at 3 or 9 months old. Altogether, the ELISA results confirmed that both Aβ_{42}Ms and Aβ_{42}Os exist in the gastrointestinal system, and their distributions are different in APP/PS1 mice, but their levels increase with age.

Meanwhile, IP-Western blotting further confirmed the presence of Aβ_{42} in the intestine through 1F12/2C6 and

1F12/1F12 ELISA. The Aβ_{42}Os signal was only observed in jejunal lysates and colon lysates of 3-month-old APP/PS1 mice (**Figure 4D, i**). In comparison, no Aβ_{42} species were detected in 3-month-old C57BL/6J mice (**Figure 4D, ii**). Compared with 3-month-old APP/PS1 mice, the distribution of Aβ_{42}Os and Aβ_{42}Ms in 9-month-old APP/PS1 mice was quite different. In 9-month-old APP/PS1 mice, obvious Aβ_{42}Os bands were observed in the stomach, jejunum, ileum, colon, cecum, jejunum lysate,

and ileum lysate, while Aβ$_{42}$Ms levels were detected in low in the jejunum, ileum, and in high in the lysates of stomach, jejunum, and cecum (**Figure 4D, iii**). However, in age-matched C57BL/6J mice, no bands of Aβ$_{42}$Ms or/and Aβ$_{42}$Os were observed (**Figure 4D, iv**). The light chain of 1F12 was used as an internal reference to ensure that the same amount of immunomagnetic beads was added to each sample. The quantitative data of Western blotting (**Figures 4E,F**) were consistent with the 1F12/2C6 and 1F12/1F12 ELISA results (**Figures 4A–C** and **Supplementary Figures 3A–F**), indicating that both the levels of Aβ$_{42}$Ms and Aβ$_{42}$Os and their distributions in the gastrointestinal system are correlated with AD progression.

Based on the results of IP-Western blotting and sandwich ELISA, we further investigated the accumulation of insoluble Aβ plaques in the intestine because Aβ$_{42}$Ms and Aβ$_{42}$Os were the core components of amyloid plaques. The immunofluorescence assay (IFA) showed that the weak fluorescent signals of thioflavin S and Cy3-1F12 were colocalized in the duodenum of 3-month-old mice (**Figure 5**, left). However, in 9-month-old APP/PS1 mice, obvious fluorescent colocalization signals of thioflavin S and Cy3-1F12 were observed in the duodenum, ileum, and cecum, which of their fluorescence signals were significantly stronger than that of 3-month-old APP/PS1 mice (**Figure 5**, right). In comparison, in 3- or 9-month-old C57BL/6J mice, no fluorescent signals of thioflavin S and Cy3-1F12 were
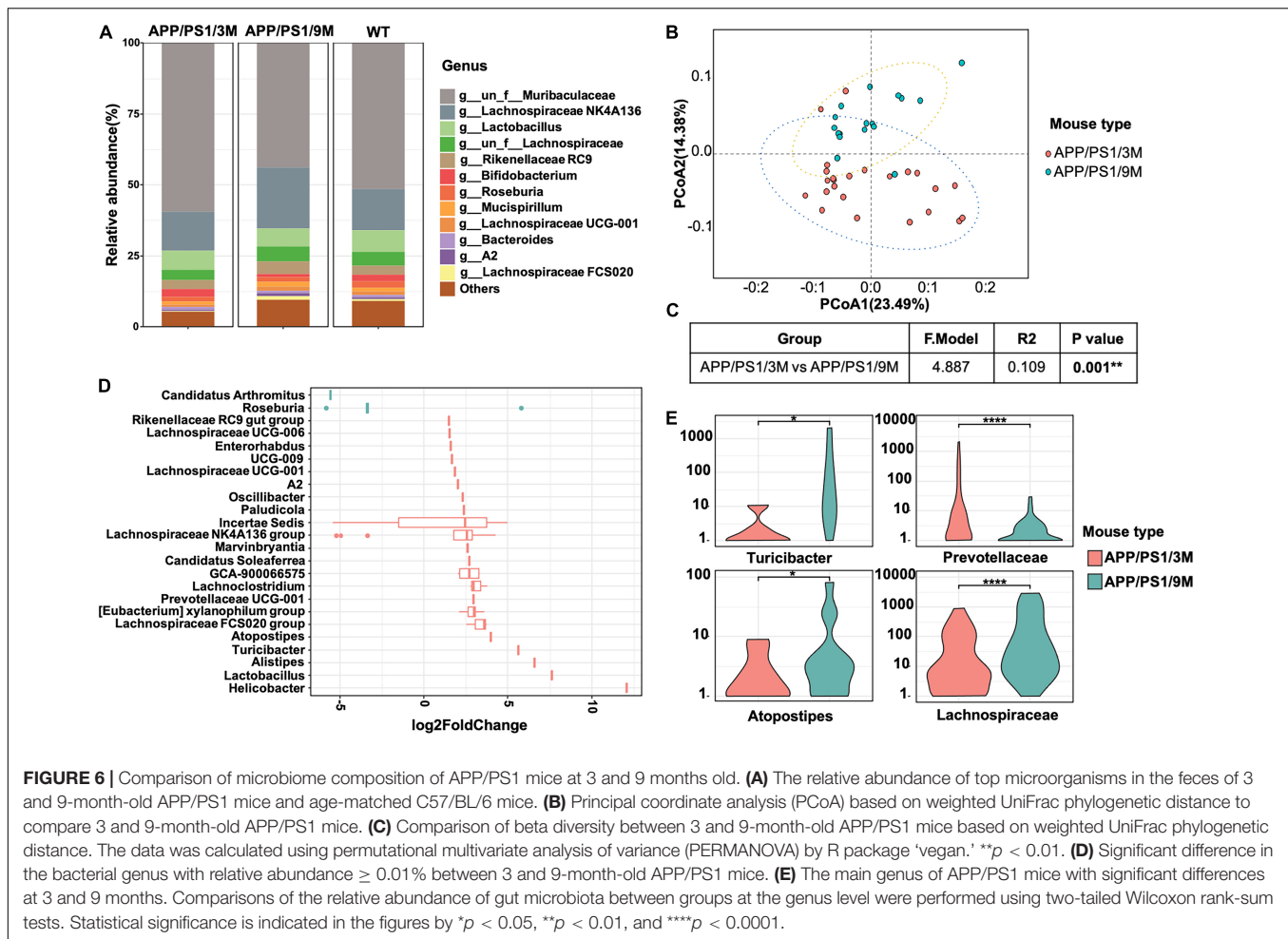
observed (**Supplementary Figure 3** and **Figure 4**). Overall, the results of sandwich ELISA (**Figures 4A–C**), IP-Western blotting (**Figure 4D**), and IFA (**Figure 5**) convincingly demonstrated that Aβ exists in the intestine of APP/PS1 mice, and their levels correlate to AD progression.

Dynamic Changes in Microbiome Composition of APP/PS1 Mice With Age

To investigate the changes in microbiome composition of APP/PS1 mice with age, we compared relative microbial abundance at genus levels among 3-month-old APP/PS1 mice, 9-month-old APP/PS1 mice, and age-matched C57BL/6J mice. Among all three groups, the abundance of Lachnospiraceae fluctuated with age (**Figure 6A**). To further characterize the microbiome composition, a beta diversity analysis was performed based on PCoA and weighted UniFrac distance in 3 and 9-month-old APP/PS1 mice (**Figure 6B**). The PERMANOVA results revealed that the microbiome structure was reshaped during the development of AD (**Figure 6C**). Then, representative bacterial taxa that differed significantly across two APP/PS1 groups were determined by 'DESeq2' R package based on the negative binomial distribution. Taxa were sorted by fold change between the two groups at the genus level (**Figure 6D**). In addition, the content of Turicibacter, Atopostipes, and
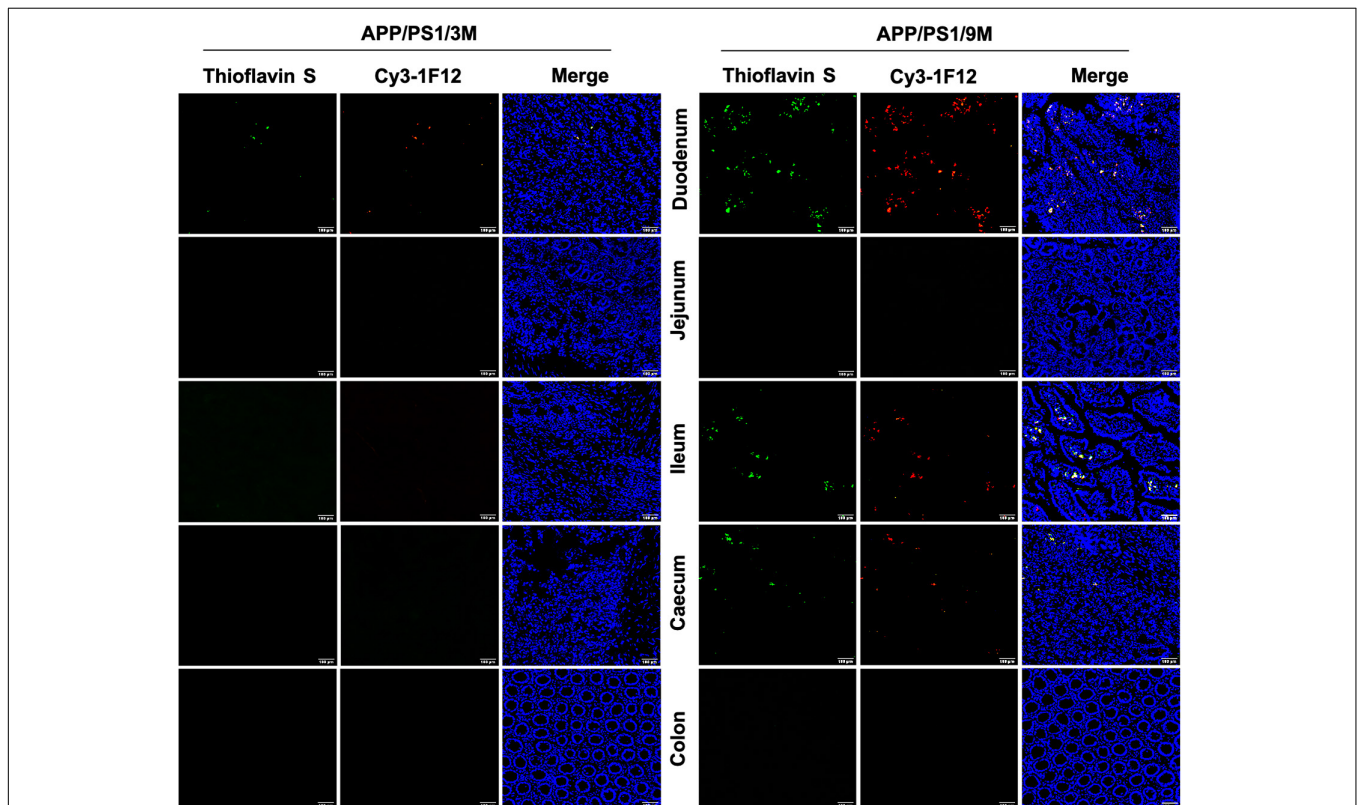
FIGURE 5 | Immunofluorescence assay for insoluble Aβ plaques in different parts of the intestines of APP/PS1 mice. The levels of insoluble Aβ plaques in the duodenum, jejunum, ileum, cecum, and colon of 3-month-old **(left)** and 9-month-old **(right)** APP/PS1 mice were evaluated by double-staining with thioflavin S and Cy3-IF12 (Scale bar: 100 μm).

FIGURE 6 | Comparison of microbiome composition of APP/PS1 mice at 3 and 9 months old. **(A)** The relative abundance of top microorganisms in the feces of 3 and 9-month-old APP/PS1 mice and age-matched C57/BL/6 mice. **(B)** Principal coordinate analysis (PCoA) based on weighted UniFrac phylogenetic distance to compare 3 and 9-month-old APP/PS1 mice. **(C)** Comparison of beta diversity between 3 and 9-month-old APP/PS1 mice based on weighted UniFrac phylogenetic distance. The data was calculated using permutational multivariate analysis of variance (PERMANOVA) by R package 'vegan.' **$p < 0.01$. **(D)** Significant difference in the bacterial genus with relative abundance $\geq 0.01\%$ between 3 and 9-month-old APP/PS1 mice. **(E)** The main genus of APP/PS1 mice with significant differences at 3 and 9 months. Comparisons of the relative abundance of gut microbiota between groups at the genus level were performed using two-tailed Wilcoxon rank-sum tests. Statistical significance is indicated in the figures by *$p < 0.05$, **$p < 0.01$, and ****$p < 0.0001$.

Lachnospiraceae in 9-month-old APP/PS1 mice was significantly higher than that in 3-month-old mice (**Figure 6E**). Meanwhile, the Prevotellaceae was less abundant in aged APP/PS1 mice (**Figure 6E**). Collectively, these results illustrated that in the early stages of AD, the composition of the gut microbiota shows a significant difference.

DISCUSSION

In this study, we screened $A\beta_{42}$ sequence- and conformation-specific antibodies 1F12 and 2C6 and selected preferred antibody pairs 1F12/2C6 and 1F12/1F12 for sandwich ELISA to accurately detect $A\beta_{42}$Ms and $A\beta_{42}$Os in blood and organs. Of note, in the results of identifying the epitopes of 1F12 and 2C6, we find that the 2C6 exhibited discrete epitopes. Presently, there are about five epitopes on the surface of $A\beta_{42}$ peptides, mainly including $A\beta_{3-9}$, $A\beta_{13-19}$, $A\beta_{18-25}$, $A\beta_{29-36}$, and $A\beta_{36-42}$ and several antibodies have been designed for the corresponding epitopes (De et al., 2019). Interestingly, our prepared 2C6 can recognize the $A\beta_{3-9}$, $A\beta_{13-19}$, $A\beta_{18-25}$, $A\beta_{29-36}$, but not for $A\beta_{36-42}$. In the detailed analysis of the immune response of $A\beta_{36-42}$, we used the keyhole limpet hemocyanin-coupled $A\beta_{36-42}$ peptides

to immunize BALB/c mice, but only one of three mice showed a weak immune response with a low titer. The inadequate immune response may be due to the $A\beta_{36-42}$ peptides (VGGVVIA) containing many hydrophobic amino acids, such as V, I, and A, making it difficult for animals to absorb and followed to produce antibodies. Therefore, the explanation of why 2C6 exhibits discrete epitopes is that there are more hydrophilic or neutral amino acids instead of hydrophobic amino acids in the region of $A\beta_{1-36}$, making it easier to be exposed and recognized by antibodies. Besides, the successful preparation of mAb A8978 (against the intermediate epitope $A\beta_{13-28}$) and mAb 78 (against $A\beta_{7-11}$, $A\beta_{18-24}$, and $A\beta_{26-32}$) indicate that it is possible to generate multiple epitope antibodies in the $A\beta_{1-36}$ region (Hatami et al., 2014; Nabers et al., 2018), and all these results also further confirm our explanation. Studies describing the different roles of $A\beta_{42}$ sequence region in the toxicity mechanisms have been reported by several groups. In general, the C-terminal area of $A\beta_{42}$ plays a significant role in inducing bilayer permeability (De et al., 2019), while the middle and N-terminal parts of $A\beta_{42}$ are effective in causing microglial inflammation and TLR signaling (Colvin et al., 2017; De et al., 2019). Therefore, antibodies targeting the C-terminal region of $A\beta_{42}$ are more effective in reducing membrane

permeability induced by $A\beta_{42}$ aggregates, whereas antibodies targeting the middle and N-terminal areas of $A\beta_{42}$ are more potent in reducing the inflammatory response induced by $A\beta_{42}$ aggregates. These differences may be due to the accessibility of solvent-exposed N-terminal fragments in larger aggregates formed in the later stages of $A\beta_{42}$ aggregation. Altogether, the functional effect of antibodies with more epitopes may be far greater than that of single-epitope antibodies, especially in terms of immunotherapy.

The 1F12/2C6 and 1F12/1F12 ELISAs provided sufficient sensitivity to detect the levels of $A\beta_{42}$Ms and $A\beta_{42}$Os in blood and tissue extracts of APP/PS1 mice, and the results were not affected by the peripheral expression of APP or $A\beta_{40}$ because the prepared 1F12 and 2C6 showed more preference for $A\beta_{42}$ species. The results of ELISA and immunoprecipitation (IP) performed in blood and brain extracts of 3- and 9-month-old APP/PS1 mice well confirmed that no APP protein brand was observed or detected, except for $A\beta_{42}$Ms and several small $A\beta_{42}$Os (**Figures 1D**, **2C,E**, **3D,E**). Longitudinal studies of blood $A\beta_{42}$Ms and $A\beta_{42}$Os levels showed extensive temporal variation within and among APP/PS1 mice that participated in our research. Based on the 1F12/2C6 and 1F12/1F12 ELISA tests, it was found that the decrease in the levels of total $A\beta_{42}$ in blood was accompanied by its increase in the brain, but total $A\beta_{42}$ levels in blood were not correlated with AD progression ($p = 0.2146$, **Figure 3A**). The results are unexpectedly consistent with the literature on $A\beta_{42}$ detection because the $A\beta_{42}$ level in previous reports did not show a significant change (Hoglund et al., 2005) using a pair of antibodies that recognize different $A\beta_{42}$ epitopes, which is similar to 1F12/2C6 ELISA. In contrast, soluble $A\beta_{42}$Os, whose levels are elevated in AD patients, are easily mis-detected in the measurement of $A\beta_{42}$, resulting in underestimation of $A\beta_{42}$Ms level and poor performance in assessing the progression of AD (Yang et al., 2013; Liu et al., 2017). However, based on our method, we found obvious decrease in the level of $A\beta_{42}$Ms and significantly increased level of $A\beta_{42}$Os in blood, and prominently elevated level of $A\beta_{42}$Os in the brains of 3 and 9-month-old APP/PS1 mice (**Figures 3B,C**). Therefore, the levels of $A\beta_{42}$Ms and $A\beta_{42}$Os in blood and brain are closely associated with AD progression, which is helpful for us to further understanding of the pathogenesis of AD.

Increasing evidence indicates that the intestine or intestinal flora is associated with the progression of AD. However, to date, almost no literature directly reports the presence of $A\beta_{42}$ in the intestinal tissues and further elaborates the relationship between $A\beta_{42}$ in the intestine and AD progression. Our study showed that significantly increased levels of $A\beta_{42}$ were observed in the gastrointestinal organs (including stomach, jejunum, ileum, colon, cecum, jejunum lysate, ileal lysate, and cecum lysate) of 9-month-old APP/PS1 mice but not in 3-month-old APP/PS1 mice or age-matched C57BL/6J mice (**Figures 4**, **5**). The level of $A\beta_{42}$Ms in the blood and brain of 3-month-old APP/PS1 mice was significantly higher than that in the intestine, indicating that the human $A\beta$ produced by APP/PS1 mice is mainly distributed in the blood and brain. While the increasing $A\beta_{42}$ levels in the gastrointestinal organs still needed more evidence to confirm whether it originates from the brain or/and

blood. Presently, several potential mechanisms of how brain $A\beta$ is released into peripheral tissues have been mentioned. Some convincing evidence suggests that brain-derived soluble $A\beta_{42}$Ms and $A\beta_{42}$Os can be absorbed by neurons and enter the intestine along the vagus nerve (Foley et al., 2020). In contrast, the administration of $A\beta_{42}$ into the gastrointestinal tract may induce amyloidosis in the central nervous system (CNS) and AD-related pathologies, such as dementia (Sun et al., 2020). Besides, a study provided by Cintron et al. (2015) demonstrated the ability of peripheral monocytes to transport $A\beta_{42}$ aggregates from the abdominal cavity to the brain, spleen, and liver. Several other groups claimed that $A\beta$ seeds could be transported via axons (Clavaguera et al., 2014; Guo and Lee, 2014; Boluda et al., 2015; Ye et al., 2015). In addition, the levels of $A\beta_{42}$ in the peripheral blood neuronal-derived exosomes in AD patients were higher than those in aMCI and healthy people, indicating that exosomes could also act as transport vehicles for $A\beta_{42}$ (Jia et al., 2019; Lakshmi et al., 2020). Altogether, neurons, axons, neuronal-derived exosomes, and peripheral monocytes can be used as potential carriers of $A\beta_{42}$ delivery, and there is currently evidence supporting axonal transport as a critical mode of disease propagation within the nervous system. In addition to the brain, other non-neural tissues, including the pancreas, kidney, spleen, heart, liver, testis, aorta, lung, skin, adrenal glands, and thyroid, also express amyloid-β protein precursor (APP). It is worth noting that the peripheral expression of APP will have the opportunity to be hydrolyzed to produce $A\beta_{42}$ when APP is transferred to its resident site tans-Golgi network (TGN), where β- and γ-secretase are distributed (Roher et al., 2009; Querfurth and LaFerla, 2010; Sakono and Zako, 2010; Hodson, 2018). The produced $A\beta_{42}$ is recycled to the cell membrane surface, which may increase the level of $A\beta_{42}$ in peripheral tissues. However, to date, it is difficult to evaluate the impact of APP produced by peripheral tissues on $A\beta$ levels in the brain and blood. The current evidence supports the brain as the primary source of $A\beta$ pools because $A\beta$ levels are the highest. Whether the source of APP or/and $A\beta$ in peripheral tissues contributes to the $A\beta$ pool of brain, blood or gastrointestinal organs and its influence on the detection of $A\beta_{42}$ levels in the brain and blood need to be further confirmed to clarify.

In a detailed analysis of the intestinal origin of $A\beta_{42}$, we found that $A\beta_{42}$Ms and $A\beta_{42}$Os were first detected in colonic lysates of 3-month-old APP/PS1 (**Figures 4B–D, i**). Interestingly, this phenomenon is partly consistent with the study reported by Hui et al. (2012) that the colon is considered the first segment of the gastrointestinal tract where $A\beta$ deposits occur. This phenomenon may be explained that in the early stage of AD, the $A\beta_{42}$, especially $A\beta_{42}$ monomers or small oligomers from the brain and blood pools, can be easily transmitted through the enteric nervous system (ENS) to the digestive tract of the stomach and intestines. According to reports, the colon contains the most neurons (Gershon, 1998; Rao and Gershon, 2016; Brierley et al., 2018; Borgmann et al., 2021), and the monomers that gradually accumulate in the colon can be aggregated into small molecular weight oligomers. It is worth noting that the colon undergoes vital processes to ensure our health. These processes are coordinated by transmitting sensory signals from the periphery to the central

nervous system, allowing communication from the intestine to the brain via the "gut-brain axis" (Brierley et al., 2018). Foley et al. (2020) have confirmed that soluble $A\beta_{42}Ms$ and $A\beta_{42}Os$ could be absorbed by neurons and enter the intestine along the vagus nerve. Therefore, there is a strong correlation between the colon and degenerative neurological disease. In general, our results and previous evidence may well explain the observation of $A\beta_{42}$ in colon lysates, but the precise correlation of $A\beta_{42}$ and the intestine still needs to be studied. Besides, the intestine and enteric nervous systems play an important role in neurological disorders and deserve our attention.

Compared to 3-month-old APP/PS1, we did not observe an increase in $A\beta_{42}$ peptides in colonic lysates, although the levels of $A\beta_{42}Ms$ and $A\beta_{42}Os$ increased sharply in 9-month-old APP/PS1 (**Figures 4B–D, iii**). The significant difference in $A\beta_{42}$ levels in colonic lysates of 3- and 9-month-old APP/PS1 mice may be due to the migration of $A\beta_{42}$ in the colon from the colon to other gastrointestinal organs. This migration process has been confirmed by multiple groups (Cintron et al., 2015; Sun et al., 2020). In addition, high $A\beta_{42}$ levels were detected in the cecum, ileum, jejunum, and even stomach of 9-month-old APP/PS1 mice. Among them, the $A\beta_{42}$ level in the ileum was more significant and higher than that in the colon or colon lysate. These results further confirmed the ability of $A\beta_{42}$ peptides to spread in the colon as seeds. Thus, the disappeared $A\beta_{42}$ peptide in the colonic lysate of 9-month-old APP/PS1 may have migrated to other gastrointestinal organs such as the cecum, ileum, jejunum, and stomach because their $A\beta_{42}$ levels were significantly higher than colon lysates. In summary, our study, together with previous studies, confirms the ability of $A\beta_{42}$ peptides to spread as seeds, which leads to extensive changes in $A\beta_{42}$ levels within and between different APP/PS1 mice.

In this study, we monitored the dynamic changes of $A\beta_{42}Ms$ and $A\beta_{42}Os$ levels in the intestines and studied their significance for AD. Indeed, our results convincingly demonstrated that $A\beta$ exists in the intestines of APP/PS1 mice, and their levels are correlated with AD progression. However, a current controversy is whether the gastrointestinal organs can directly produce $A\beta_{42}$. Several studies have reported that microorganisms including *Bacillus subtilis*, *Shigella*, *Escherichia coli*, *Salmonella enterica*, *Staphylococcus aureus*, and *Mycobacterium tuberculosis* can produce functional extracellular amyloid proteins but not for $A\beta_{42}$ peptides (Hufnagel et al., 2013; Schwartz and Boles, 2013; Friedland, 2015; Pistollato et al., 2016). In fact, it seems that there is insufficient evidence to show that $A\beta_{42}$ peptides could be directly produced in the organs of the gastrointestinal tract. In addition, the practical and accurate distinction between locally produced and transported $A\beta_{42}$ peptides is crucial for helping to understand the pathology of AD. Distinguishing the local production and transportation of $A\beta_{42}$ peptides is our next research plan.

In addition to finding elevated levels of soluble $A\beta_{42}$, several insoluble $A\beta_{42}$ plaques were observed in the intestines of 3-month-old APP/PS1 mice. However, it is in the early stages of AD, and there were only a few plaques in the brain (**Figure 5**, left). With the progression of AD, more plaques were observed in the intestines of 9-month-old APP/PS1 mice (**Figure 5**, right).

Interestingly, changes in microbiome composition were observed in 9-month-old APP/PS1 mice. The effect of increased levels of $A\beta_{42}$ in the intestine on the changes in its microbial composition remains obscure. There is no doubt that the observed toxicity of $A\beta_{42}$, especially small oligomers, is the most effective in inducing inflammation of microglia or macrophages, and it causes more damage in inducing bilayer permeability (Flagmeier et al., 2017; Fusco et al., 2017; De et al., 2019). It is certain that in the current investigation, the abundance of Lachnospiraceae fluctuated with age (**Figures 6C,D**). The content of Turicibacter, Atopostipes, and Lachnospiraceae in aged APP/PS1 mice was significantly higher than in young APP/PS1 mice, but the abundance of Prevotellaceae in old APP/PS1 mice was lower (**Figure 6**). Overall, these results indicated that the significant difference in gut microbiota composition is accompanied by the sharply increased soluble $A\beta_{42}$ and insoluble $A\beta$ plaques during AD progression, but whether this change affects or is affected by the change in gut-derived $A\beta_{42}$ needs to be further explored.

In summary, based on our screened antibody pairs 1F12/2C6 and 1F12/1F12 in sandwich ELISA for specific detection of $A\beta_{42}Ms$ and $A\beta_{42}Os$, we observed apparent fluctuation in the levels of $A\beta_{42}Ms$ and $A\beta_{42}Os$ in blood and intestines of APP/PS1 mice during the progression of AD. The identification of $A\beta_{42}$ abnormalities in the gastrointestinal tract could provide new ideas for AD therapeutic interventions that are only used to evaluate $A\beta_{42}$ levels in peripheral blood and the brain. Furthermore, studying the relationship between the levels of $A\beta_{42}Ms$ and $A\beta_{42}Os$ in peripheral tissues and the progression of AD may help to understand the causes of AD, and may provide new treatment strategies for improving AD or other $A\beta$-related dementias.

DATA AVAILABILITY STATEMENT

The datasets presented in this study can be found in online repositories. The names of the repository/repositories and accession number(s) can be found in the article.

ETHICS STATEMENT

The animal study was reviewed and approved by the Institutional Animal Care and Use Committee of Huazhong University of Science and Technology.

AUTHOR CONTRIBUTIONS

HL, QL, and ZZ coordinated the writing of the manuscript and provided writing guidance and manuscript revision. LZ completed all experiments and contributed to writing the first draft. YL and SN participated in most experiments. XL was involved in APP/PS1 mice breeding and schematic figure preparations. CY performed the bioinformatics data analysis. All authors reviewed and approved the final manuscript.

FUNDING

ACKNOWLEDGMENTS

SUPPLEMENTARY MATERIAL

The Supplementary Material for this article can be found online at: https://www.frontiersin.org/articles/10.3389/fnmol.2021.723317/full#supplementary-material

Supplementary Figure 1 | Characterization of sequence- and conformation-specific antibodies 1F12 and 2C6 against Aβ_{42}Ms and Aβ_{42}Os.

(A) The preferred hybridoma colonies were screened via indirect ELISA. **(B)** The purity and molecular weight of purified 1F12, 2C6, and 2E2 were confirmed via 12% reduced SDS-PAGE with Coomassie blue staining. **(C)** The bioactivities of 1F12, 2C6, and commercial antibody 6E10 toward natural Aβ_{42} peptides extracted from murine APP/PS1 brain were evaluated via Western blotting. **(D)** Confocal fluorescence images of murine APP/PS1 brain sections using Cy3-labeled anti-Aβ_{42} monoclonal antibody 2C6 and commercially available anti-Aβ antibody 6E10 **(E)**. (Scale bar: 200 μm). **(E)** Titers of 1F12, 2C6, and 2E2. **(F)** The purity and molecular weight of freshly prepared Aβ_{42}Ms and Aβ_{42}Os were determined by Western blotting with 2C6. **(G)** Binding affinities of 2C6 toward Aβ_{42}Ms and Aβ_{42}Os were evaluated via indirect ELISA. The activities **(H)** and titers **(I)** of the biotinylated 1F12 or 2C6 antibody.

Supplementary Figure 2 | Confocal fluorescence images of whole murine APP/PS1 brain sections using Cy3-labeled anti-Aβ_{42} monoclonal antibody 1F12 **(A)** or 2C6 **(B)** and thioflavin S.

Supplementary Figure 3 | Comparison of the dynamic distribution of Aβ_{42} in APP/PS1 and C57BL/6J. The levels of total Aβ_{42} **(A,D)**, Aβ_{42}Os **(B,E)**, and Aβ_{42}Ms **(C,F)** in the stomach, duodenum, jejunum, ileum, colon, and cecum and their lysates from APP/PS1 and C57BL/6J at 3-month-old (n = 4) or 9-month-old APP/PS1 (n = 4). Data are presented as means ± SEM. Two-way analysis of variance (ANOVA) was used for multigroup comparisons. Statistical significance is indicated in the figures by **$p < 0.01$, ***$p < 0.001$ and ****$p < 0.0001$.

Supplementary Figure 4 | Representative confocal fluorescence images of the duodenum, jejunum, ileum, cecum, and colon of 3-month-old C57BL/6J mice double-stained with thioflavin S and Cy3-1F12 (Scale bar: 100 μm).

Supplementary Figure 5 | Representative confocal fluorescence images of the duodenum, jejunum, ileum, cecum, and colon of 9-month-old C57BL/6J mice double-stained with thioflavin S and Cy3-1F12 (Scale bar: 100 μm).

REFERENCES

Benilova, I., Karran, E., and De Strooper, B. (2012). The toxic Aβ oligomer and Alzheimer's disease: an emperor in need of clothes. *Nat. Neurosci.* 15, 349–357. doi: 10.1038/nn.3028

Bernstein, S. L., Dupuis, N. F., Lazo, N. D., Wyttenbach, T., Condron, M. M., Bitan, G., et al. (2009). Amyloid-beta protein oligomerization and the importance of tetramers and dodecamers in the aetiology of Alzheimer's disease. *Nat. Chem.* 1, 326–331. doi: 10.1038/nchem.247

Boluda, S., Iba, M., Zhang, B., Raible, K. M., Lee, V. M., and Trojanowski, J. Q. (2015). Differential induction and spread of tau pathology in young PS19 tau transgenic mice following intracerebral injections of pathological tau from Alzheimer's disease or corticobasal degeneration brains. *Acta Neuropathol.* 129, 221–237. doi: 10.1007/s00401-014-1373-0

Borgmann, D., Ciglieri, E., Biglari, N., Brandt, C., Cremer, A. L., Backes, H., et al. (2021). Gut-brain communication by distinct sensory neurons differently controls feeding and glucose metabolism. *Cell Metab.* 33, 1466–1482.e1467. doi: 10.1016/j.cmet.2021.05.002

Brierley, S. M., Hibberd, T. J., and Spencer, N. J. (2018). Spinal afferent innervation of the colon and rectum. *Front. Cell. Neurosci.* 12:467. doi: 10.3389/fncel.2018.00467

Cintron, A. F., Dalal, N. V., Dooyema, J., Betarbet, R., and Walker, L. C. (2015). Transport of cargo from periphery to brain by circulating monocytes. *Brain Res.* 1622, 328–338. doi: 10.1016/j.brainres.2015.06.047

Clavaguera, F., Grueninger, F., and Tolnay, M. (2014). Intercellular transfer of tau aggregates and spreading of tau pathology: implications for therapeutic strategies. *Neuropharmacology* 76 (Pt A), 9–15. doi: 10.1016/j.neuropharm.2013.08.037

Collaborators, G. B. D. D. (2019). Global, regional, and national burden of Alzheimer's disease and other dementias, 1990-2016: a systematic analysis for the Global Burden of Disease Study 2016. *Lancet Neurol.* 18, 88–106. doi: 10.1016/S1474-4422(18)30403-4

Colvin, B. A., Rogers, V. A., Kulas, J. A., Ridgway, E. A., Amtashar, F. S., Combs, C. K., et al. (2017). The conformational epitope for a new Aβ42 protofibril-selective antibody partially overlaps with the peptide N-terminal region. *J. Neurochem.* 143, 736–749. doi: 10.1111/jnc.14211

De, S., Wirthensohn, D. C., Flagmeier, P., Hughes, C., Aprile, F. A., Ruggeri, F. S., et al. (2019). Different soluble aggregates of Aβ42 can give rise to cellular toxicity through different mechanisms. *Nat. Commun.* 10:1541. doi: 10.1038/s41467-019-09477-3

Driscoll, I., Resnick, S. M., Troncoso, J. C., An, Y., O'brien, R., and Zonderman, A. B. (2006). Impact of Alzheimer's pathology on cognitive trajectories in nondemented elderly. *Ann. Neurol.* 60, 688–695. doi: 10.1002/ana.21031

Flagmeier, P., De, S., Wirthensohn, D. C., Lee, S. F., Vincke, C., Muyldermans, S., et al. (2017). Ultrasensitive measurement of Ca(2+) influx into lipid vesicles induced by protein aggregates. *Angew. Chem. Int. Ed Engl.* 56, 7750–7754. doi: 10.1002/anie.201700966

Foley, A. R., Roseman, G. P., Chan, K., Smart, A., Finn, T. S., Yang, K., et al. (2020). Evidence for aggregation-independent, PrP(C)-mediated Aβ cellular internalization. *Proc. Natl. Acad. Sci. U.S.A.* 117, 28625–28631. doi: 10.1073/pnas.2009238117

Friedland, R. P. (2015). Mechanisms of molecular mimicry involving the microbiota in neurodegeneration. *J. Alzheimers Dis.* 45, 349–362. doi: 10.3233/jad-142841

Fusco, G., Chen, S. W., Williamson, P. T. F., Cascella, R., Perni, M., Jarvis, J. A., et al. (2017). Structural basis of membrane disruption and cellular toxicity by α-synuclein oligomers. *Science* 358, 1440–1443. doi: 10.1126/science.aan6160

Gershon, M. D. (1998). *The Second Brain: The Scientific Basis of Gut Instinct.* New York, NY: Harper Collins.

Gu, L., and Guo, Z. (2013). Alzheimer's Abeta42 and Abeta40 peptides form interlaced amyloid fibrils. *J. Neurochem.* 126, 305–311. doi: 10.1111/jnc.12202

Guo, J. L., and Lee, V. M. (2014). Cell-to-cell transmission of pathogenic proteins in neurodegenerative diseases. *Nat. Med.* 20, 130–138. doi: 10.1038/nm.3457

Harach, T., Marungruang, N., Duthilleul, N., Cheatham, V., Mc Coy, K. D., Frisoni, G., et al. (2017). Reduction of Abeta amyloid pathology in APPPS1 transgenic mice in the absence of gut microbiota. *Sci. Rep.* 7:41802. doi: 10.1038/srep41802

Hatami, A., Albay, R. III, Monjazeb, S., Milton, S., and Glabe, C. (2014). Monoclonal antibodies against Aβ42 fibrils distinguish multiple aggregation

state polymorphisms in vitro and in Alzheimer disease brain. *J. Biol. Chem.* 289, 32131–32143. doi: 10.1074/jbc.M114.594846

Hodson, R. (2018). Alzheimer's disease. *Nature* 559:S1. doi: 10.1038/d41586-018-05717-6

Hoglund, K., Thelen, K. M., Syversen, S., Sjogren, M., Von Bergmann, K., Wallin, A., et al. (2005). The effect of simvastatin treatment on the amyloid precursor protein and brain cholesterol metabolism in patients with Alzheimer's disease. *Dement. Geriatr. Cogn. Disord.* 19, 256–265. doi: 10.1159/000084550

Hong, K. S., and Yaqub, M. A. (2019). Application of functional near-infrared spectroscopy in the healthcare industry. *J. Inn. Opt. Health Sci.* 12. doi: 10.1142/S179354581930012X

Hu, X., Wang, T., and Jin, F. (2016). Alzheimer's disease and gut microbiota. *Sci. China Life Sci.* 59, 1006–1023. doi: 10.1007/s11427-016-5083-9

Hufnagel, D. A., Tükel, C., and Chapman, M. R. (2013). Disease to dirt: the biology of microbial amyloids. *PLoS Pathog* 9:e1003740. doi: 10.1371/journal.ppat.1003740

Hui, L., Chen, X., and Geiger, J. D. (2012). Endolysosome involvement in LDL cholesterol-induced Alzheimer's disease-like pathology in primary cultured neurons. *Life Sci.* 91, 1159–1168. doi: 10.1016/j.lfs.2012.04.039

Jia, L., Qiu, Q., Zhang, H., Chu, L., Du, Y., Zhang, J., et al. (2019). Concordance between the assessment of Aβ42, T-tau, and P-T181-tau in peripheral blood neuronal-derived exosomes and cerebrospinal fluid. *Alzheimers Dement.* 15, 1071–1080. doi: 10.1016/j.jalz.2019.05.002

Jiang, C., Li, G., Huang, P., Liu, Z., and Zhao, B. (2017). The gut microbiota and Alzheimer's disease. *J. Alzheimers Dis.* 58, 1–15. doi: 10.3233/jad-161141

Kim, K. M., Jang, H. C., and Lim, S. (2016). Differences among skeletal muscle mass indices derived from height-, weight-, and body mass index-adjusted models in assessing sarcopenia. *Korean J. Intern. Med.* 31, 643–650. doi: 10.3904/kjim.2016.015

Kohler, G., and Milstein, C. (1975). Continuous cultures of fused cells secreting antibody of predefined specificity. *Nature* 256, 495–497. doi: 10.1038/256495a0

Lakshmi, S., Essa, M. M., Hartman, R. E., Guillemin, G. J., Sivan, S., and Elumalai, P. (2020). Exosomes in Alzheimer's disease: potential role as pathological mediators, biomarkers and therapeutic targets. *Neurochem. Res.* 45, 2553–2559. doi: 10.1007/s11064-020-03111-1

Liu, L., Chang, Y., Yu, J., Jiang, M., and Xia, N. (2017). Two-in-one polydopamine nanospheres for fluorescent determination of beta-amyloid oligomers and inhibition of beta-amyloid aggregation. *Sens. Actuators B Chem.* 251, 359–365.

Mancuso, C., and Santangelo, R. (2018). Alzheimer's disease and gut microbiota modifications: the long way between preclinical studies and clinical evidence. *Pharmacol. Res.* 129, 329–336. doi: 10.1016/j.phrs.2017.12.009

Mucke, L., and Selkoe, D. J. (2012). Neurotoxicity of amyloid beta-protein: synaptic and network dysfunction. *Cold Spring Harb. Perspect. Med.* 2:a006338. doi: 10.1101/cshperspect.a006338

Murphy, M. P., and LeVine, H. III (2010). Alzheimer's disease and the amyloid-beta peptide. *J. Alzheimers Dis.* 19, 311–323. doi: 10.3233/JAD-2010-1221

Nabers, A., Perna, L., Lange, J., Mons, U., Schartner, J., Güldenhaupt, J., et al. (2018). Amyloid blood biomarker detects Alzheimer's disease. *EMBO Mol. Med.* 10:e8763. doi: 10.15252/emmm.201708763

Nag, S., Sarkar, B., Bandyopadhyay, A., Sahoo, B., Sreenivasan, V. K., Kombrabail, M., et al. (2011). Nature of the amyloid-beta monomer and the monomer-oligomer equilibrium. *J. Biol. Chem.* 286, 13827–13833. doi: 10.1074/jbc.M110.199885

Naslund, J., Haroutunian, V., Mohs, R., Davis, K. L., Davies, P., Greengard, P., et al. (2000). Correlation between elevated levels of amyloid beta-peptide in the brain and cognitive decline. *JAMA* 283, 1571–1577. doi: 10.1001/jama.283.12.1571

Oxtoby, N. P., Young, A. L., Cash, D. M., Benzinger, T. L. S., Fagan, A. M., Morris, J. C., et al. (2018). Data-driven models of dominantly-inherited Alzheimer's disease progression. *Brain* 141, 1529–1544. doi: 10.1093/brain/awy050

Pistollato, F., Sumalla Cano, S., Elio, I., Masias Vergara, M., Giampieri, F., and Battino, M. (2016). Role of gut microbiota and nutrients in amyloid formation and pathogenesis of Alzheimer disease. *Nutr. Rev.* 74, 624–634. doi: 10.1093/nutrit/nuw023

Querfurth, H. W., and LaFerla, F. M. (2010). Alzheimer's disease. *N. Engl. J. Med.* 362, 329–344. doi: 10.1056/NEJMra0909142

Rao, M., and Gershon, M. D. (2016). The bowel and beyond: the enteric nervous system in neurological disorders. *Nat. Rev. Gastroenterol. Hepatol.* 13, 517–528. doi: 10.1038/nrgastro.2016.107

Roberts, K. F., Elbert, D. L., Kasten, T. P., Patterson, B. W., Sigurdson, W. C., Connors, R. E., et al. (2014). Amyloid-beta efflux from the central nervous system into the plasma. *Ann. Neurol.* 76, 837–844. doi: 10.1002/ana.24270

Roher, A. E., Esh, C. L., Kokjohn, T. A., Castano, E. M., Van Vickle, G. D., Kalback, W. M., et al. (2009). Amyloid beta peptides in human plasma and tissues and their significance for Alzheimer's disease. *Alzheimers Dement.* 5, 18–29. doi: 10.1016/j.jalz.2008.10.004

Sakono, M., and Zako, T. (2010). Amyloid oligomers: formation and toxicity of Abeta oligomers. *FEBS J.* 277, 1348–1358. doi: 10.1111/j.1742-4658.2010.07568.x

Salminen, A., Ojala, J., Suuronen, T., Kaarniranta, K., and Kauppinen, A. (2008). Amyloid-beta oligomers set fire to inflammasomes and induce Alzheimer's pathology. *J. Cell. Mol. Med.* 12, 2255–2262. doi: 10.1111/j.1582-4934.2008.00496.x

Schwartz, K., and Boles, B. R. (2013). Microbial amyloids–functions and interactions within the host. *Curr. Opin. Microbiol.* 16, 93–99. doi: 10.1016/j.mib.2012.12.001

Sperling, R. A., Aisen, P. S., Beckett, L. A., Bennett, D. A., Craft, S., Fagan, A. M., et al. (2011). Toward defining the preclinical stages of Alzheimer's disease: recommendations from the National Institute on Aging-Alzheimer's Association workgroups on diagnostic guidelines for Alzheimer's disease. *Alzheimers Dement.* 7, 280–292. doi: 10.1016/j.jalz.2011.03.003

Sun, Y., Sommerville, N. R., Liu, J. Y. H., Ngan, M. P., Poon, D., Ponomarev, E. D., et al. (2020). Intra-gastrointestinal amyloid-β1-42 oligomers perturb enteric function and induce Alzheimer's disease pathology. *J. Physiol.* 598, 4209–4223. doi: 10.1113/jp279919

Wang, W., Hou, T. T., Jia, L. F., Wu, Q. Q., Quan, M. N., and Jia, J. P. (2019). Toxic amyloid-beta oligomers induced self-replication in astrocytes triggering neuronal injury. *EBioMedicine* 42, 174–187. doi: 10.1016/j.ebiom.2019.03.049

Wang, X., Sun, G., Feng, T., Zhang, J., Huang, X., Wang, T., et al. (2019). Sodium oligomannate therapeutically remodels gut microbiota and suppresses gut bacterial amino acids-shaped neuroinflammation to inhibit Alzheimer's disease progression. *Cell Res.* 29, 787–803. doi: 10.1038/s41422-019-0216-x

Wang, Y. J., Zhou, H. D., and Zhou, X. F. (2006). Clearance of amyloid-beta in Alzheimer's disease: progress, problems and perspectives. *Drug Discov. Today* 11, 931–938. doi: 10.1016/j.drudis.2006.08.004

Xiang, Y., Bu, X. L., Liu, Y. H., Zhu, C., Shen, L. L., Jiao, S. S., et al. (2015). Physiological amyloid-beta clearance in the periphery and its therapeutic potential for Alzheimer's disease. *Acta Neuropathol.* 130, 487–499. doi: 10.1007/s00401-015-1477-1

Yang, T., Hong, S., O'malley, T., Sperling, R. A., Walsh, D. M., and Selkoe, D. J. (2013). New ELISAs with high specificity for soluble oligomers of amyloid β-protein detect natural Aβ oligomers in human brain but not CSF. *Alzheimers Dement.* 9, 99–112.

Ye, L., Hamaguchi, T., Fritschi, S. K., Eisele, Y. S., Obermüller, U., Jucker, M., et al. (2015). Progression of seed-induced Aβ deposition within the limbic connectome. *Brain Pathol.* 25, 743–752. doi: 10.1111/bpa.12252

Zhang, L., Wei, Q., Han, Q., Chen, Q., Tai, W., Zhang, J., et al. (2018). Detection of *Shigella* in milk and clinical samples by magnetic immunocaptured-loop-mediated isothermal amplification assay. *Front. Microbiol.* 9:94. doi: 10.3389/fmicb.2018.00094